

Journal Pre-proof

Study on the characterisation of the PTFE transfer film and the dimensional designing of surface texturing in a dry-lubricated bearing system

Liang Ding, Dragos Axinte, Paul Butler-Smith, A.M. Abdelhafeez



PII: S0043-1648(19)31718-1

DOI: <https://doi.org/10.1016/j.wear.2020.203238>

Reference: WEA 203238

To appear in: *Wear*

Received Date: 25 November 2019

Revised Date: 23 January 2020

Accepted Date: 11 February 2020

Please cite this article as: L. Ding, D. Axinte, P. Butler-Smith, A.M. Abdelhafeez, Study on the characterisation of the PTFE transfer film and the dimensional designing of surface texturing in a dry-lubricated bearing system, *Wear* (2020), doi: <https://doi.org/10.1016/j.wear.2020.203238>.

This is a PDF file of an article that has undergone enhancements after acceptance, such as the addition of a cover page and metadata, and formatting for readability, but it is not yet the definitive version of record. This version will undergo additional copyediting, typesetting and review before it is published in its final form, but we are providing this version to give early visibility of the article. Please note that, during the production process, errors may be discovered which could affect the content, and all legal disclaimers that apply to the journal pertain.

© 2020 Published by Elsevier B.V.

Study on the characterisation of the PTFE transfer film and the dimensional designing of surface texturing in a dry-lubricated bearing system

Liang Ding, Dragos Axinte*, Paul Butler-Smith, AM Abdelhafeez

Machining and Condition Monitoring Group, Faculty of Engineering, University of Nottingham, NG7 2RD, UK

Abstract

The ability of polytetrafluoroethylene (PTFE) to form tribo-film in dry sliding condition makes it a popular liner material for self-maintenance bearings, such as those in the helicopter main and tail rotors. Nowadays, hard fillers or reinforcing-fibres are added to form the PTFE composite with enhanced strength and wear resistance; however, this also leads to increasing possibility of wear tracks on counter-surface and therefore more difficulty in observing and characterising the transfer film. In this paper, a surface analysis method based on using SEM analysis, supplemented with a Time-of-flight Secondary-ion mass spectrometry (ToF-SIMS) techniques for calibration was developed to give a comprehensive view of the transfer film formation on bearing steel surfaces. Previous challenges in transfer film identification and characterisation were also pinpointed. A series of laser surface textures (dimples), designed for improving the tribological performance of the bearing were tested, and the effects on transfer film formation have been evaluated by the surface analysis method. It is found that the depth of the dimples should match with the thickness of the transfer film to achieve a benefiting effect of the film formation, while the diameter and the coverage of the textures needs to be relatively small to avoid a high level of abrasion.

Keywords: PTFE composite; transfer film; surface analysis; surface texturing

1 Introduction

Self-lubricated bearings, in which dry lubricants are impregnated to replace external lubricant supply, are widely used in engineering applications where frequent maintenance is difficult and fluid lubricating plant is challenging to implement. For example, for corrosion-resistant powertrain where a continuous operation is essential [1], Molybdenum disulphide (MoS_2) journal bearings are used [2], and for artificial joints which needs to be implanted in human bodies for years, Ultra-High Molecular Weight Polyethylene (UHMWPE) spherical bearings are adopted [3]. Another instance that faces similar issue is the helicopter main and tail rotors, as the overall cost for ceasing the flight and servicing is dramatic [4], and light-weight design is needed for ever-increasing demand for higher speed. Therefore, the helicopter rotor-heads are generally equipped with self-lubricating bearings functioning by Polytetrafluoroethylene (PTFE), a low-friction self-lubricating polymer. Apart from PTFE, the bearing liner composite also contains reinforcing material such as Kevlar and glass fibre to improve wear resistance. Similar with the MoS_2 and UHMWPE, it has been proven that, the self-lubricating property of PTFE is fulfilled by the transfer film formation on the metallic surface during sliding contact [5–7]. The formation and functioning of the transfer film are then found influenced by the topography and physical properties of the counter-surface. For instance, in previous research, it was found that the hardness of the counter-surface [8], the value of the average roughness (Ra) [9] and the pattern of the roughness (from different finishing process) can all have a great impact on the formation of transfer film, which consequently affects the wear performance of the bearings [10]. Therefore, when studying the tribological effects of a

modification technology on the counter-surface, the analysis on its influence on the transfer film has always been the key element to illustrate the mechanism how it may alter the frictional and wear performance of the bearings. Nevertheless, it seems there has never been a consensus on how to establish a systematic observation of the transfer film. Early studies on the PTFE transfer films used optical techniques such as interference microscopy [11] and ellipsometry [12], utilising respectively the optical path difference (OPD) and the change in polarisation to estimate the thickness of the transfer film. The film thickness was calculated to be at most hundreds of nanometres in most contact conditions, while in some high speed applications (>1 m/s) thicker sheets and lumps can be built [13]. However, these optical methods require the counter-surface to be considerably smooth, so that the transfer film, rather than the substrate's surface can predominantly induce the optical effects. Similarly, measurements by Atomic Force Microscopy [14] are also prone to be influenced by the substrate's roughness. Therefore, in most of these methods, the observations on the counter-surfaces were limited to ultra-smooth glass or silicon wafer, and only pure PTFE were tested to avoid wear on counter-surface. With the development of PTFE composite, more hard-fillers or stiffening fibres have been added to increase the strength and wear resistance of the composite, thus inevitably leading to wear-tracks on counter-surface. As a result, using optical techniques for identifying and characterising transfer film become ineffective.

To solve the problem of identifying transfer film, various more advanced technologies have been used. For example, X-ray photoelectron spectroscopy (XPS) was employed to characterise the PTFE transfer formed in rolling-sliding [15]. The interpretation of the results from XPS was not so straightforward though, as the film coverage was calculated indirectly using a set of film-thickness-values reported in other literature. SEM is a more commonly used surface analysis method, adopted by many researchers for characterising PTFE transfer films [16,17]. However, in some occasions, difficulties could be experienced in identifying the PTFE transfer film precisely with SEM. For example, in a study on the formation of the transfer film on steel surfaces [18], it was found that the film coverage revealed by SEM was very different from the one by Time-of-flight Secondary-ion mass spectrometry (ToF-SIMS) [18], a reliable technology for identifying thin-film as it only sputters monolayers from the surface. This issue in SEM observation is probably caused by the high penetration depths, estimated to be a few micro-meters depending on the composition of the metallic surfaces [19] under normally adopted accelerating voltages (15 to 25 keV). Therefore if the transfer film is as some postulated [12] (i.e. just monolayers or nano-metres thick), the information of it can be overwhelmingly surpassed by the substrate below.

Because of the difficulty in accurately observing the PTFE transfer film, particularly the inefficiency in assessing its features, e.g. thickness, the development in the modifying the counter-surface using surface texturing technology has been hindered. As found by Singh, the particle size and the thickness of transfer film of dry lubricants should match with the surface topographic variations to ensure its function [20]. Therefore, without a reliable method to identify the transfer film and measure its thickness in different conditions, the surface modifications tend to be conservative, and thus, normally constrained within altering smaller-scale features like surface roughness [9].

The study on the tribological performance of artificially textured surface can date back to Hamilton et al.'s work in 1966 [21]. In this study, micro-asperities were produced on mechanical seals by an etching technique, and the dimensions were optimised theoretically

and experimentally. After that, various surface texturing techniques have progressed, such as vibro-machining [22] and vapour deposition techniques [23]. After the Etsion' work on laser-textured seal surface [24], the research on laser-surface-texturing also saw a boom. Nowadays, industrialised applications include honing on the engines' cylinder walls for lubricant reservation, and micro-texturing in MEMS for prevention of adhesion and stiction.

Although the surface textures are more frequently applied in fluid-lubricated condition, in which they serve as micro-bearings[25,26], C. Gachot [27,28] reported that in dry-sliding, the textures can also create beneficial effects like altering stress distribution. However, it has been noticed that, many reported benefiting textures in dry-contact are applied under low loading condition [29–31]. This is mainly because that textures in dry-contact inherently increase the contact stress [32], thus magnifying the adverse effects of surface texturing such as increasing hysteresis resistance [10] and micro-cutting [33]. However, textures also have the potential of boosting the formation of transfer film for some dry-lubricated contact, as the dry lubricant film in this occasion can also be stored by the textures. As a result, the induced overall influence on the frictional and wear performance of the dry-lubricated bearings would be the result of the combination of the different effects incurred (e.g. micro-abrasion and lubricant reservation). In addition, the weighing of these effects and alteration of related tribological phenomena can be dependent on texturing dimensions, as analogous phenomena have been observed in previous research on the surface roughness. Taking the study from Kennedy et al. [34] as an example, it was found that the variation of the wear life of polyethylene is a result of the combined effects of friction and third body film thickness. Consequently, the turning point where rougher surface can contribute to higher wear life is where the substantial third body film can be reserved between asperities to reduce the resistance. Given this, a comprehensive surface analysis is again essential for studying the effects of surface texturing, since analysis on the coverage and morphology of wear debris and transfer film is a good indication for the occurring tribological phenomenon.

To address these challenges, the present paper focuses on the development of a systematic observation and characterisation method for transfer film of dry-lubricant, and the application of this method to explore whether the beneficial or detrimental effects would be induced by surface texturing on the transfer film formation. Moreover, special attention is given to the measurement of the transfer film thickness, whose relation with the dimensions of the surface textures would give an indication whether the benefiting effect of lubricant reservation would become prominent.

2 Test methodology

Due to their nature as solids, dry lubricants are commonly used in applications where requirement for load-carry-capacity is high, but operational sliding speed is relatively low. The spherical plain bearing used in helicopter's rotors, for example, is a typical application. In flight conditions, the pitch-control bearings are driven by the actuators, going through swivelling rotation constrained within 15° oscillation angle (occasionally tilting within 5° in main rotors) [35]. Normally, the resultant nominal contact pressure is between 10 and 40 MPa, and the relative sliding speed ranges from 0.01 to 0.15 m/s. With these working conditions considered, the pin-on-plate reciprocating sliding wear test is capable of reproducing the sliding contact conditions. In addition, based on the application scenario, this section also presents the techniques used to establish the novel characterisation method for

the transfer film and to observe the tribological phenomena, together with the development of a FEA model as an assistance to analyse the wear mechanism. In this paper, it is aimed to use the methodologies to evaluate the both the tribological performance and the transfer film formation under different texturing dimensions and coverages, and to understand the phenomena behind the influence from these variables of texturing.

2.1 Sample preparation

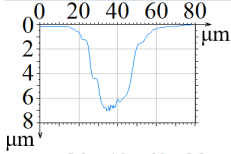
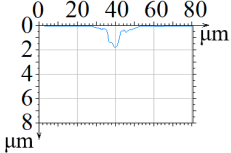
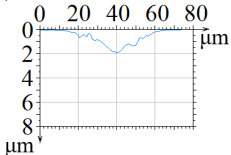
The pin sample used in the wear test is the X1 PTFE/glass fibre woven fabric composite (bounded by phenolic resin), which is widely used as the bearing liner in modern helicopter rotor-heads. Each sample has the same thickness of 280 μ m and square surface area of 7 mm \times 7 mm.

The counter-surface is the AMS5630 440C stainless steel, with the hardness of 56 HRC. The average surface roughness is around R_q 0.02 μ m in its original state. Ekspla AtlanticHE 1064 pico-second pulsed laser (pulse duration 50 pico-seconds, estimated peak fluence 73.98 J/cm² and wavelength of 1064 nm) is used for generating bespoke texturing patterns on the counter-surface. During laser ablation, a heat affected zone (HAZ) arises near the ablated area as a results of heat diffusion, along with thermal effects such as oxidation layer (occasionally with micro-cracks). Moreover, it should be noticed that the grain refinement and hardening due to local quenching may boost the occurrence of micro-abrasion during contact. However the influence is likely to be minor with pico-second laser, as both the theoretical estimation (diffusion length around 20nm judging from equation in [36]) and the observation on similar cases (pico-second laser on stainless steel) [37] indicate a minimal HAZ. Even though the laser is capable of producing complex texturing forms, such as ellipse holes and grooves (linear or curved), these forms can induce influencing factors like aspect ratio and trench orientation, whose impacts can be particularly significant considering the anisotropic properties of the composite liner. However, the focus of the study is on the effects on the transfer film phenomena from the textures' basic dimensions (depth, width/diameter and area coverage). Therefore, uniformly distributed circular concavity is proposed to be the form applied on the counter-surface to minimize the influence from directional influencing factors. Moreover, preliminary trials with relatively large holes (diameter > 60 μ m) or coverages (merely higher than 10%) ended up with extremely fast wear-out and failure of liner, so the texture pattern is further confined to dimples (created by single laser shots) with diameters ($d = 20, 40 \mu\text{m}$) and coverage percentages ($p_c = 0.4\%, 1.6\%$ and 6.4%) as shown in Table 1.

To study the effects of dimple depth, particularly its relation with the transfer film's thickness (later revealed in Section 3.2.1), a dimple depth considerably larger than the maximum film thickness is adopted in Type A, while a depth shallower than the maximum thickness is proposed for dimple B and C for comparison. Meanwhile, for Type B dimples, the diameter is reduced to half of the original dimples created by the laser, so that its comparison with Type A and C can include effects of dimples' diameters. Therefore, from Type A-C, the three types of dimples constitute relatively the 'wide & deep' (A), 'narrow & shallow' (B) and 'wide & shallow' (C) textures. Since the Type B dimple's diameter is half of A and C's, the settings of the coverage percentages can lead to that the distance for Type B dimples at a certain coverage (e.g. 0.4%) can equalise with that of Type A or C dimples in the higher coverage (e.g. 1.6%). Benefiting from it, in later analysis of the influence from dimples' spacing densities, whether it attributes to distance or area coverage can be recognised. For a

more straightforward presentation, the three levels of texture coverage are later referred as ‘low’ (0.4%), ‘medium’ (1.6 %) and ‘high’ (6.4 %).

Table 1. Matrix of dimensions and texturing coverage percentage of surface textures to test

Dimple type		Coverage p_c (Percentage of dimpled area)		
A - Wide & deep ($d=40\mu\text{m}$, $Dep=8\mu\text{m}$)		Low	Medium	High
		(0.4%)	(1.6%)	(6.4%)
B - Narrow & shallow ($d=20\mu\text{m}$, $Dep=2\mu\text{m}$)		Low	Medium	High
		(0.4%)	(1.6%)	(6.4%)
C - Wide & shallow ($d=40\mu\text{m}$, $Dep=2\mu\text{m}$)		Low	Medium	High
		(0.4%)	(1.6%)	(6.4%)

To generate the proposed different groups of textured steel surfaces the reference group of smooth steel surfaces, the processing of the steel plates follow three main steps (**Fig. 1**): laser dimpling on the original smooth surface; first polishing step (using Struers LaboSystem machine and a polishing cloth with 1 μm -diameter grits) to remove the inherent material re-deposition, and final polishing to round the dimple edges.

To achieve the different coverages designated in Table 1, the spacing L between the adjacent dimples need to be set before the texturing step following the equation:

$$L = \sqrt{\frac{\pi d_1^2}{4p_c}} \quad (1)$$

where d_1 is the diameter of the dimples, and p_c is the desired coverage percent of the dimples.

What should be noticed is that d_1 should be the diameter of the dimples after the final step. Therefore, d_1 is determined by both the original diameter d_0 (determined by the laser beam) of the dimples by laser shots, and the reduction in diameter as the dimple gets shallower during the first polishing step (influence from the final step is negligible). Considering this, two calibration procedures need to be done before the process. Firstly, the relationship between the dimensions of the original dimples (diameter d_0 and depth Dep) and the parameters of the laser (power P and dwell time t_l , step 1 in Fig. 1) needs to be found. Then, the polishing parameters (normal force N , rotating speed ω and time t_p , step 2 in Fig. 1) to achieve the polishing depth in the first polishing process should be determined. Therefore, the diameter d_1 , as well as the dimple depth Dep after the final step could be obtained by controlling the processing variables stated above.

In this test series, the laser dimpling process was conducted utilising single laser shots on evenly spaced points with the output power of 6 W and repetition rate of 30 kHz. By controlling the laser dwell time (t_l), dimples with different depth (Dep) can be produced ($t_l =$

10 milliseconds for $Dep = 8 \mu\text{m}$ and $t_l = 4$ milliseconds for $Dep = 3 \mu\text{m}$). Meanwhile, a 2D galvanometer head with a 4-axis stage (Aerotech system) with the positioning precision of $0.1 \mu\text{m}$, was used for manoeuvring the distance (L) between the laser shots to achieve different covering percentage of dimples. After the first step, dimples with fixed initial diameter d_0 (related to the diameter of the laser beam, i.e. $40 \mu\text{m}$) were created. Then, with 40N normal force and 200RPM rotating speed set on the polishing machine, the surfaces were polished shortly ($t_p = 1$ minute) if the desired diameter is $40 \mu\text{m}$ (Type A or C), or for longer ($t_p = 6$ minutes) if a $20 \mu\text{m}$ diameter is to be achieved (Type B).

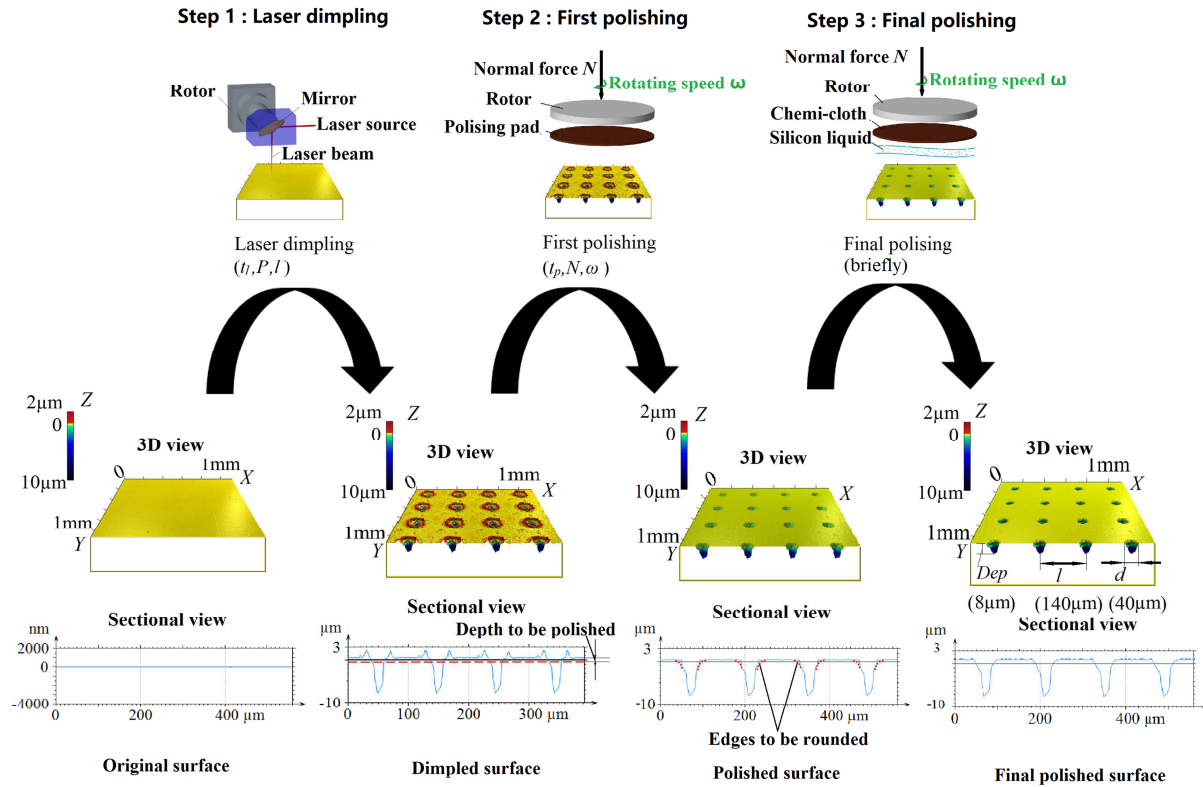


Fig. 1. Processing scheme for manufacturing the textured surface

After the first polishing step, the dimples would often be left with sharp edges. In the authors' experience, they may act as micro-cutting edges during sliding which leads to accelerated wear of the PTFE counterpart composite. To prevent this, the sample surfaces were polished for around 10 seconds using MetPrep final polishing cloth and $0.05 \mu\text{m}$ silica suspension, just to round the dimples' edges with little influence to their dimensions.

Similarly, the un-textured steel samples, which would be used as the reference smooth surfaces, were put under the same batch for the two polishing steps, so that the same surface roughness ($R_q 0.015 \mu\text{m}$) can be obtained.

2.2 Sliding wear test

In order to simulate the oscillating sliding contact in the pitch-control bearings of the real helicopter rotor-heads, linear reciprocating motion is produced through the crank-slider system in a modified BICERI universal wear test machine (Fig. 2(a)). In the tests conducted, the rotating speed of the rotor was set at 180 RPM (i.e. 3 Hz reciprocating frequency), and the reciprocating stroke length was set as 20 mm . As for the load, a 196 N normal force was

applied using weights. With this set-up, the pressure-velocity factor achieved (average sliding speed 0.12 m/s, and nominal contact pressure 40 MPa) are similar to those occurring in the bearings of the real helicopter rotor-heads.

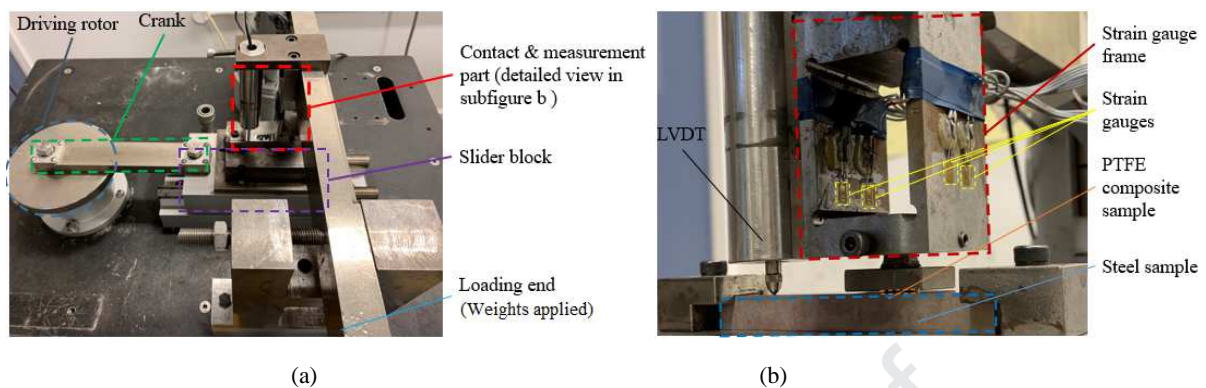


Fig. 2. Images of (a) set-up of the reciprocating sliding wear test rig and (b) detailed view of the contact & measurement part

The measurement of the friction force has been performed using two full bridges of strain gauges (Vishay L2A-06-062LW-120) bonded on the rectangular shear frame (**Fig. 2(b)**). As for the wear rate, in order to achieve a continuous measurement without interruption of the tests, a Linear Variable Differential Transformer (LVDT) was implemented vertically, while the probe is in contact with the steel sample at the bottom to measure the descending of the lever incurred by the wear of the liner.

2.3 Novel approach for analysis of transfer film

To address the issues in observing and characterising the PTFE transfer film, and to develop a new method aiming at reliable observation and comprehensive characterisation the PTFE transfer film, varied techniques have been tested and presented for surface analysis in this study.

Firstly, a Keyence VH-7000 portable microscope is used for direct optical observations.

Then, to allow the influence from surface topography to be taken into consideration, a Bruker Contour GT-I 3D Optical interferometer is employed to obtain the surface topographic images.

As for the SEM analysis, in order to overcome the difficulties of accurately observing the PTFE film, we have proposed here firstly to test the imaging under different, particularly low accelerating voltages to cover the information of PTFE transfer film in different thickness. Meanwhile another surface analysis would be used as a reference for ‘calibration’, to ensure the information of the thin film has been thoroughly covered. In this study, the ToF-SIMS can be a reliable ‘calibration’ method, as it involves elemental analysis, and has the strength on characterising thin films. In turn, the calibrated SEM analysis can compensate the SIMS’ drawbacks, namely it is destructive (to the top molecule-layers) and much more time-consuming.

In this study, a FEI Quanta 650 ESEM is used to acquire both SE and BSE images, while ToF-SIMS IV (ION-ToF GmbH) instrument utilising a Bi primary ion source was employed to obtain different ion mappings. Corresponding to the SEM series with different accelerating voltages, the electrons’ trajectories are simulated through CASINO v2.5, a

commercial Monte-Carlo simulation software, to gain the information depth in each condition, giving estimation of the film thickness.

With the transfer film characterisation method comprehensively developed, it is further employed in the surface analysis for the dimensions' effects of surface texturing.

2.4 Finite element analysis for understanding of contact phenomena

To help explaining the possible effects induced by varying dimensions (e.g. diameter, depth) of surface texturing, a Finite Element (FE) model was developed in Abaqus/CAE 2016 to enable the correlation of the phenomena occurring during the tribological tests with the theory of contact mechanics. Special attention was given to the effects like micro-cutting and plastic-deformation caused by stress concentration, and the difference drawn from variation in dimple dimensions (e.g. diameter and depth).

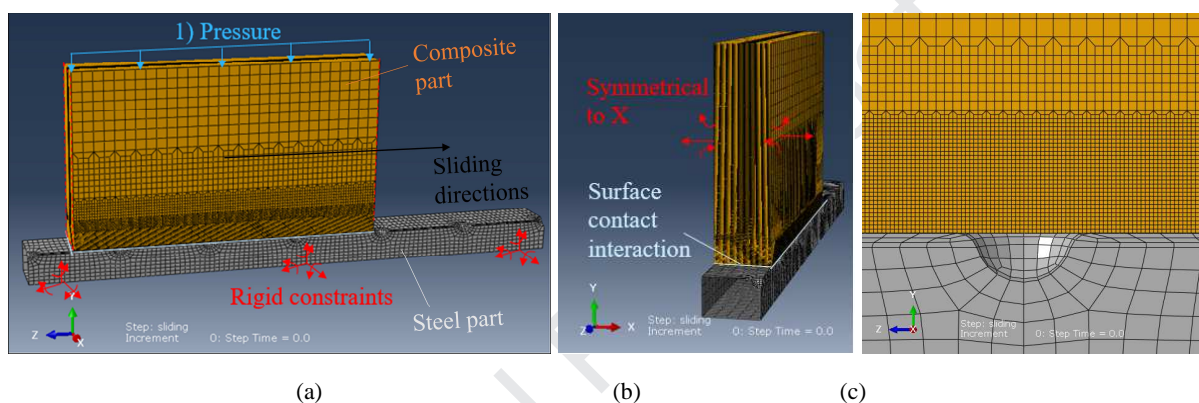


Fig. 3. Demonstration of (a) geometric models, loading conditions and boundary conditions (b) interactions applied; (c) transition of the grid size (magnified view)

To simulate the frictional contact between the contact pair, the composite (in orange) and the steel counterparts (in grey) have been connected with a surface contact interaction (**Fig. 3(b)**), while the frictional properties (i.e. coefficient of friction (CoF)) is acquired from the wear tests conducted. In addition, to improve the computational efficiency, considering the symmetrical arrangement of the model's geometry and the uniform normal load applied, only a small section of the two contact parts was built with symmetrical boundary condition applied on the composite's sectional surface. Finally, to ensure an economical yet accurate computation, fine grids ($1 \mu\text{m}$) were meshed near the interface (bottom of the composite), which is the area of key importance for the contact problem, while grids gradually transiting coarser ($16 \mu\text{m}$ on the very top) were meshed for upper zones (**Fig. 3(c)**).

The loading and the sliding velocity were set to completely mimic the test conditions stated in section 2.2, and the definition of mechanical properties of the composite combines its tensile test data with the approach in [38].

3 Test results and analysis

3.1 Friction and wear measurements

Firstly, a brief benchmarking test series is conducted, with the purpose of extracting the influence of reduced contact area caused by texturing. Since the nominal contact area will be reduced by correspondingly 0.4%, 1.6% and 6.4% with the three coverages of dimples

applied, the nominal contact pressure will be increased to 40.16 MPa, 40.65 MPa and 42.74 MPa (40 MPa for smooth/non-textured surface). Therefore, it is expected to experience a rise in wear rate and drop in CoF, which is a renowned feature of PTFE [5]. However, these influence on frictional and wear performance within the resultant pressure range need to be investigated, so that they can be separated from the texture's effects on other aspects (e.g. transfer film formation) in later analysis. To fulfil this, a series of tests with contact pressure slightly elevated from the designated test load (40 MPa) were conducted. For each contact pressure, 3 repeats were performed. Even though small deviations exist between repeats, the 3 conditions are still distinguishable and only a representative repeat is presented in **Fig. 4**. Consequently, as can be seen in **Fig. 4(a)**, with the contact pressure increasing from 40 MPa to 42 MPa and then 44 MPa, the CoF keeps dropping from 0.062 to around 0.058. Meanwhile for the wear resistance, the wear rates only increase slightly, which can be seen from **Fig. 4(b)**. Even though correspondingly the wear life decreases gradually from 33 hours to 31.5 hours, the drops between each interval are similar, without a sudden fall. From this benchmarking, it can be seen that the influence that will be caused by altered nominal contact pressure within this range is not dramatic.

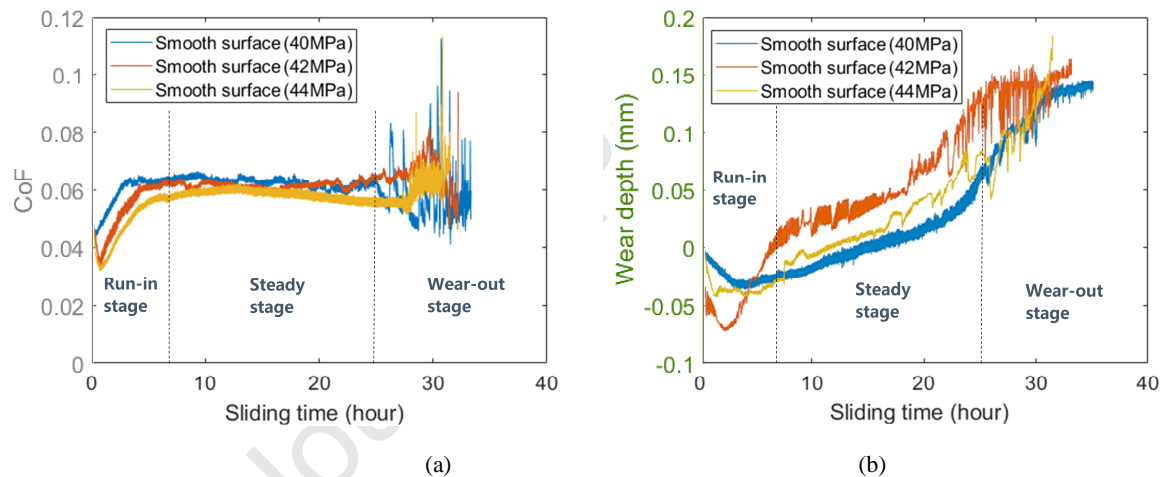


Fig. 4. Comparison of (a) coefficient of friction (CoF) and (b) wear progression of the PTFE composite sliding against smooth (i.e. non-textured) steel surfaces in different nominal contact pressures

The influence of textures with different dimensions and densities were then tested while the smooth surface (40 MPa) is used as reference. To begin with, Type A (wide & deep) dimples incur no benefit on frictional performance at any coverage, as shown in **Fig. 5(a)**, but almost doubled the steady-state CoF with the highest coverage (6.4%). As for the wear performance, it is indicated in **Fig. 5(b)** that with all but the lowest coverage (0.4%) would a remarkably worse wear performance (higher steady-state wear rate and a shorter wear life) be resulted. However, as has been tested initially (**Fig. 4**), theoretically under the elevated nominal contact pressures that the texturing coverages can lead to, the CoF should still decrease compared with the smooth surface, and the wear performance should only deteriorate marginally. Therefore, the inferior performance of the texturing patterns can only be explained by the existence of another effect, which can increase the friction and jeopardises the wear performance further.

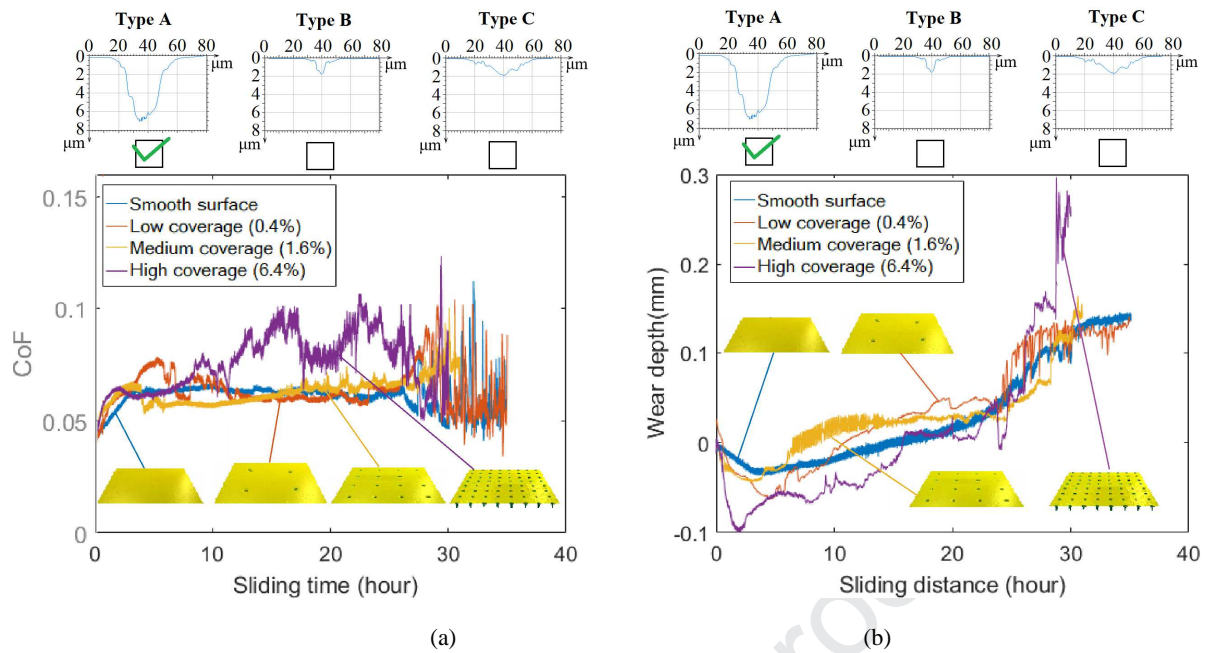


Fig. 5. Measurement of (a) friction coefficient and (b) wear progression for different coverages of Type A (wide & deep) dimples

In contrary, with the Type B dimples (narrow & shallow), improvements have been observed in both frictional and wear performance compared with the smooth surface, particularly with the medium coverage (1.6%). For example, as shown in **Fig. 6(a)**, the steady-stage frictional coefficient can be reduced by around 7% (0.005) with both the medium and high coverage. In terms of wear performance, both the low and medium coverages prolong the wear life by around 14% (5 hours), while only the medium coverage also outperforms the smooth surface substantially in terms of the wear rate at the steady stage. Therefore, it can be seen that Type B dimples (narrow & shallow) in medium coverage (1.6%) generates the most outstanding improvements in both frictional and wear performance. More importantly, the drop in CoF is more prominent than solely from the impact of increased contact pressure (curves of 42 MPa and 44 MPa in **Fig. 4(a)**), and the adverse influence on wear performance from of increased contact pressure (in **Fig. 4(b)**) has been reversed. Considering this, the beneficial texturing pattern must induce another effect other than rising contact pressure that contributes to the extra drop of CoF and wear rate.

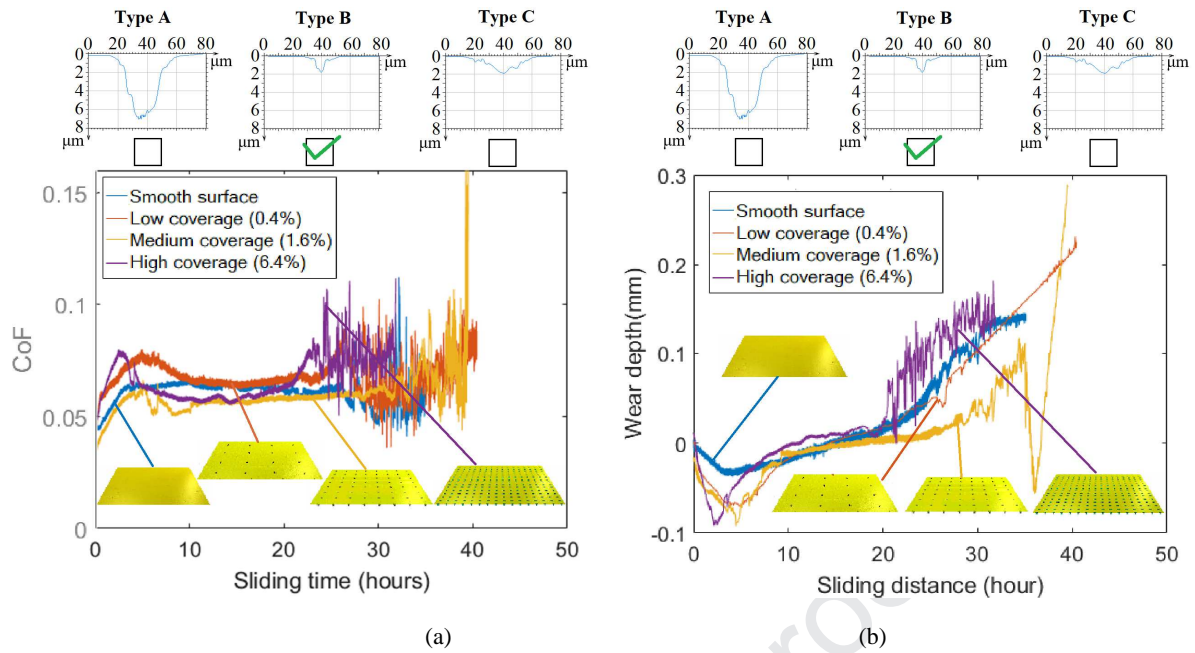


Fig. 6. Measurement of (a) friction coefficient and (b) wear progression for different coverages of Type B (narrow & shallow) dimples

Finally, with the Type C dimples (wide & shallow), both the low (0.4%) and high (6.4%) coverages exhibit no improvement on frictional performance, but incur a small degree of detriment to the wear rate and wear life, as demonstrated in Fig. 7(a) and (b). Similar with the Type B dimples (narrow & shallow), with medium coverage (1.6%) the Type C dimples (wide & shallow) can improve the wear performance with the smooth surface as the reference, even though in comparison the improvement is more marginal- the steady-stage wear rate is around 6% lower than the smooth surface and the wear life is 5% longer.

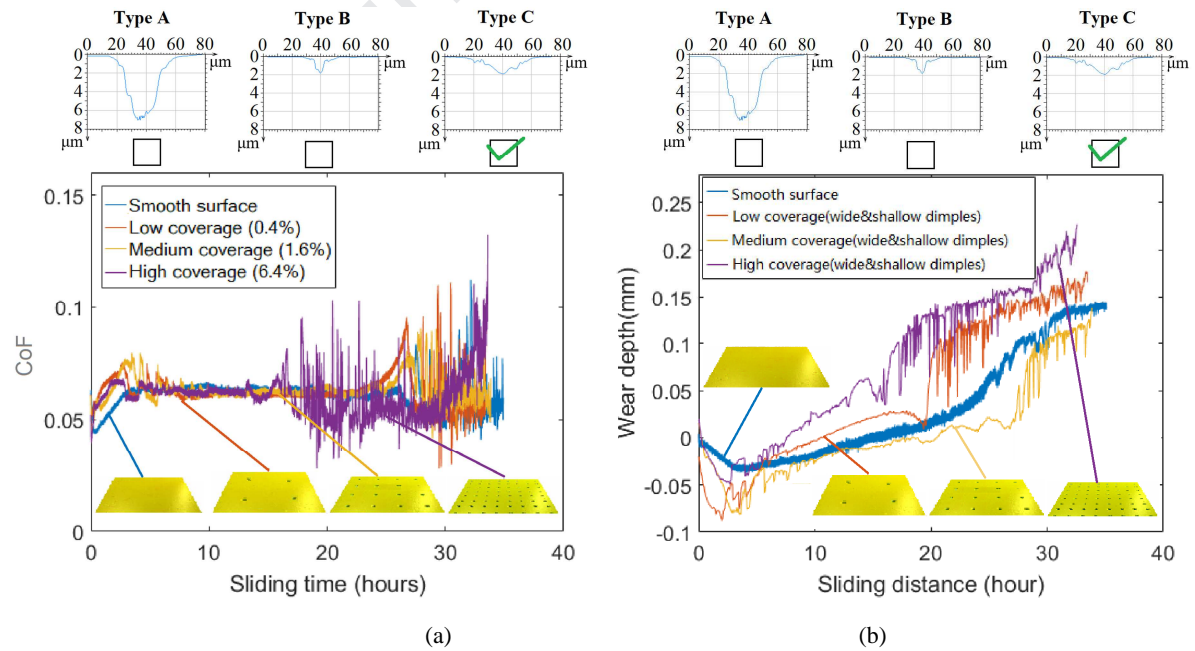


Fig. 7. Measurement of (a) friction coefficient and (b) wear progression for different coverages of Type C (wide & shallow) dimples

The frictional and wear performance are summarised in **Fig. 8**, from three repeats for each tested conditions. As can be seen, the Type A dimples (wide & deep) always bring detrimental, if not no influence on the frictional and wear performance. However, for Type B dimples (narrow & shallow) or Type C dimples (wide & shallow), there is an outstanding trend that both frictional and wear performance improve when the coverage increases from the low to the medium, but then worsened when rising further to the high. It is only with this ‘optimal’ medium coverage (1.6%) of Type B dimples (narrow & shallow), considerable improvements in frictional coefficient, wear rate and wear life can be observed.

The comments related to **Fig. 5- Fig. 8** reveal the observational influences from surface texturing on the tribological performance. Nevertheless, the governing physical phenomena inducing these different performance are the key to generate general principles analysing contact between dry-lubricating composite and textured counter-surfaces, and would be explored in the following sections.

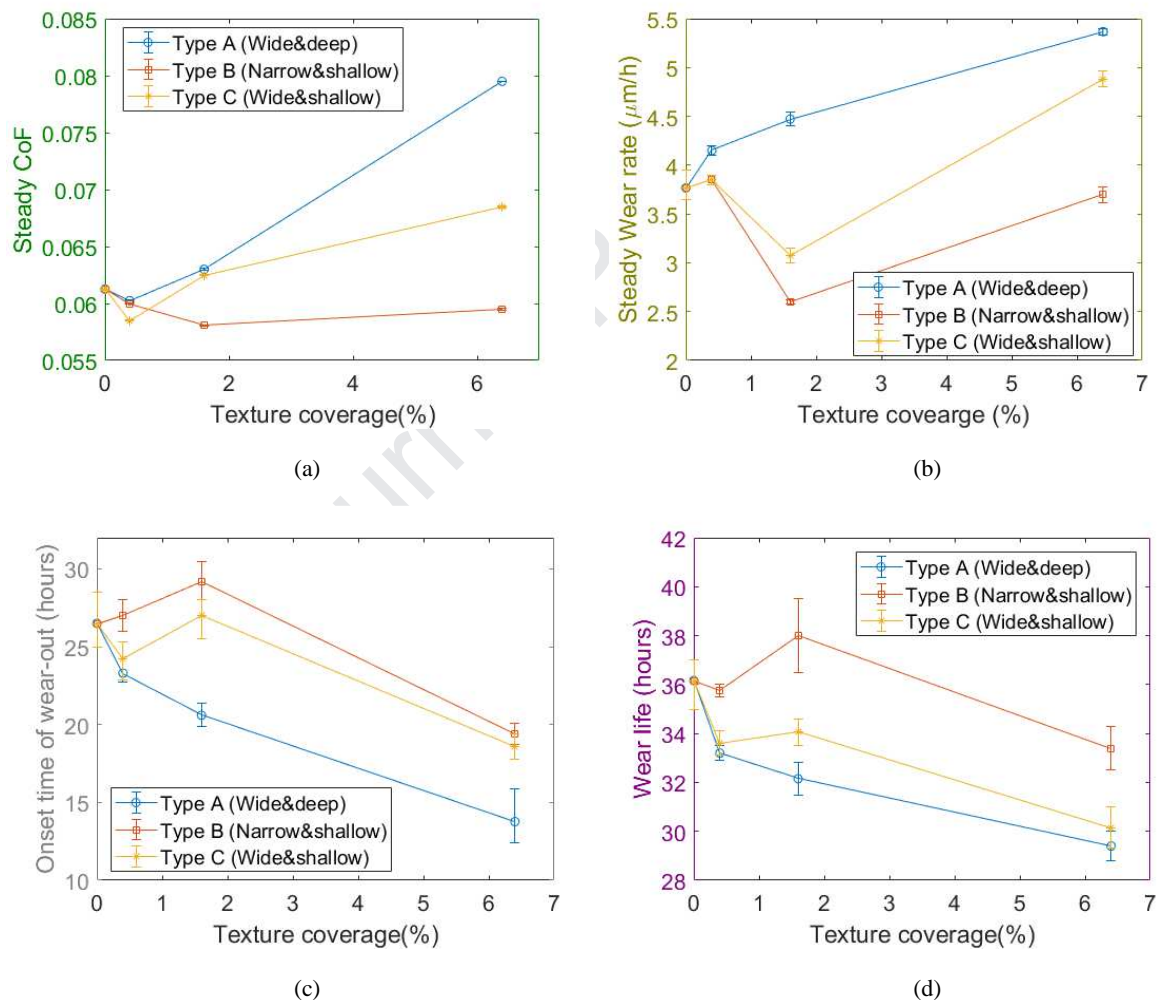


Fig. 8. Summary of (a) Steady state frictional coefficients, (b) Steady state wear rates, (c) Onset time of wear-out stage and (d) Wear life for surfaces with different texture dimensions and coverages

3.2 Surface analysis results

A thorough analysis on the counter-surface and the transfer film formation can give a good indication of the wear behaviour, assisting identification of the causes of the influence (beneficial or detrimental) found in the section (3.1) above. To perform this, a novel analysis

approach of the transfer film is firstly developed and then applied on the tested counter-surfaces.

3.2.1 Transfer film characterisation: Benchmark on smooth counter-surface

In this section, an in-depth surface analysis to identify and characterise transfer film is presented with an emphasis on the new characterisation technique (SEM analysis with varying accelerating voltages and SIMS calibration), which has been introduced in the methodology section. The surface analysis presented in this section was performed on a smooth counter-surface that has been half-way through a full wear test, to ensure a substantial formation of PTFE transfer film.

Common practice for examining PTFE transfer films with optical microscopic image (Fig. 9 (a)) is to distinguish the PTFE simply by darkness. The areas darker than a subjective 'threshold' value is marked as black and identified as PTFE transfer film when the image is converted into binary, as shown in Fig. 9(b). From the binary image, it can be seen that a large proportion of the dark area are long, thin strips along the sliding direction. However, from the surface topographic image Fig. 9 (c), it can also be seen that along the sliding direction, many scratches were also created on the counter-surface, which in practice can create the 'dark' optical effects as well. Consequently, the optical imaging would lead to exaggerated estimation of the film coverage. Meanwhile, the surface topographic image (Fig. 9(c)) is unable to reveal the transfer film accurately neither, since the topographic change is no longer just the result of transfer film, but its combination with surface wear, which in this case can be a few micrometres in depth. Overall, the methods using optical effects to identify the transfer film can be unreliable due to the presence of the wear on the counter-surface.

As proposed in the methodology section 2.3, BSE imaging in SEM analysis is a promising candidate to eliminate the uncertainties in optical methods, given that it can be validated by a reliable calibration method. To reveal its capability to detect thin film (sub-micron level), we test the BSE imaging of the transfer film on steel surface using low accelerating voltages (under 10 keV). As displayed in Fig. 10(a) and (b), some distinctive dark areas appear, corresponding to composition with smaller atomic weight in BSE images. As the accelerating voltages used for the two images are different (10 keV and 5 keV), the dark areas also differ, indicating that the layers of this low-weight material are of different thickness. In all the elemental composition of the contact samples, apart from fluorine in PTFE, elements from glass fibres (Si, O) and phenolic resin (C, H, O) are all lighter elements compared with iron (Fe), the dominant element of the steel. Moreover, if oxidation of iron manifests as a film on the surface, its overall atomic weight is also considerably smaller than iron itself. Therefore, to use the SIMS analysis to identify the composition of the dark areas becomes essential.

To clarify the identity of the dark areas, the mappings of the ions containing fluorine and other possible elements are generated for calibration using SIMS. Firstly, it can be seen that the areas with high concentration of $C_2F_4^+$ ions (bright spots in Fig. 10(c)) resemble well with the dark areas in BSE image, particularly in marked details I-IV in Fig. 10(b). Other fluorine-ions such as $C_6F_9^+$ and F^- , although not shown here, have a very similar pattern. As for the mapping of other ions, such as Si^+ and Fe^{3+} (Fig. 11 (d) and (e)), the difference with the BSE images is significant. To conclude, the BSE images' resemblance with exclusively the Fluorine ions' mapping confirms that the dark areas in the BSE images represent the transfer of PTFE. Moreover, we would like to note that this technique should not be restricted

to only PTFE transfer film, and can work for identification of other thin transfer film with featuring elements (e.g Mo4+ in MoS2).

In comparison, some of the PTFE coverages detected by SIMS image of $C_2F_4^+$ can be missing in the optical microscopic image and its binary version. For instance, areas I, V and IV in **Fig. 11** (b) are ‘flooded’ in the surface scratches and consequently the coverages are not sufficiently presented in **Fig. 10**(a).

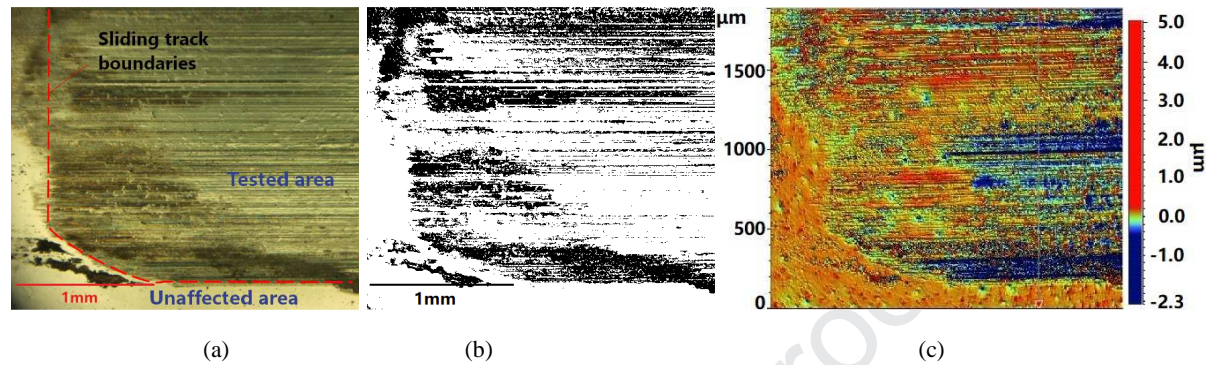


Fig. 9. Observation of the smooth (non-textured) steel counter-surface using (a) optical microscopic image, (b) binary image converted from microscopic image, and (c) surface topographic image.

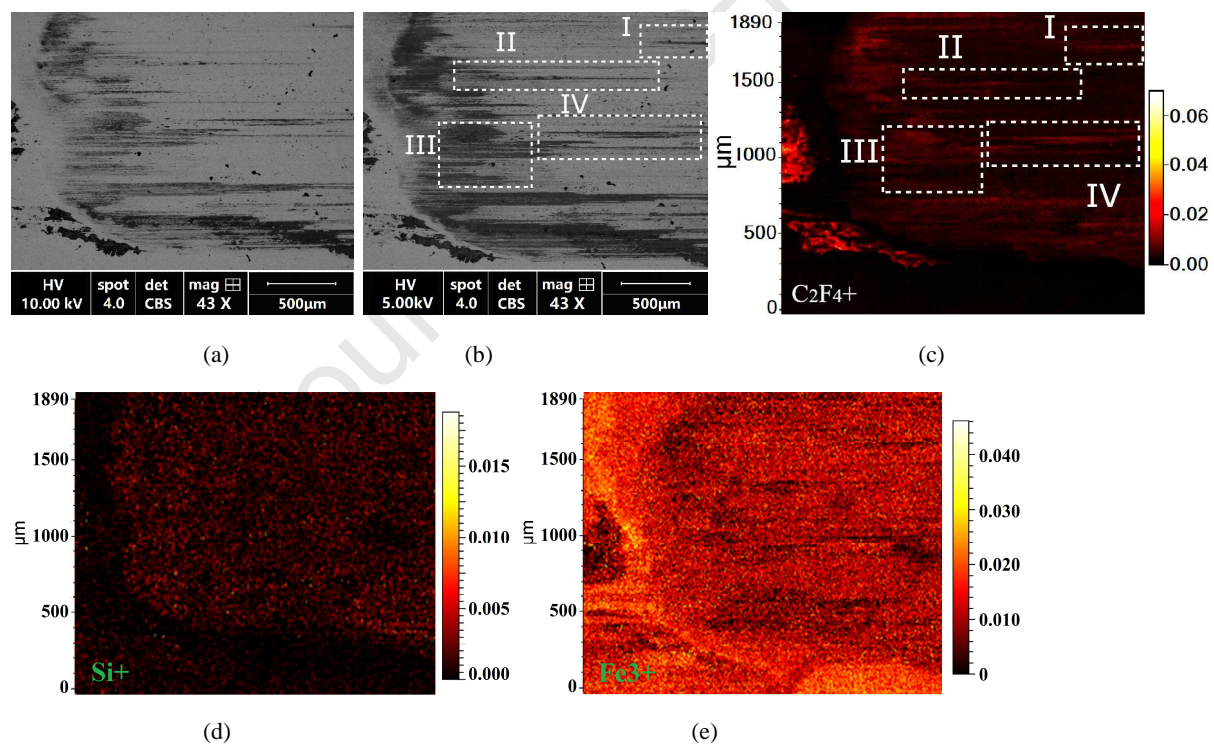


Fig. 10. Observation of smooth (non-textured) counter-surface using (a) BSE image (accelerating voltage = 10keV), (b) BSE image (accelerating voltage = 5keV), (c) SIMS image of $C_2F_4^+$ (counts normalized), (d) SIMS image of Si^+ (counts normalized), (e) SIMS image of Fe^{3+} (counts normalized).

With SEM investigation conducted on another location on the smooth surface, the acquired images **Fig. 11**. (a)- (d) give a good example how the revealed coverage of PTFE transfer film changes with accelerating voltages. Comparing **Fig. 11**(a) and (b), it can be seen that from 20 keV to 10 keV, the PTFE transfer film revealed by BSE image does not change significantly, with a long-strip-morphology along the sliding direction as the main morphology. However, when the accelerating voltage decreases to 5 keV, the detected film

coverage increases dramatically, almost occupying the whole tested steel area, as shown in **Fig. 11(c)**. This means that there is a step-change in the transfer film's thickness, from around 1 micrometre or above (maximum 2~3 μm estimated from observations under higher voltages), to only tens of nanometres considering the simulated distributions of the electrons' penetration depth (**Fig. 11(e)** to **(g)**). There is, however, not much transfer film existing in-between these thicknesses. Finally, when the accelerating voltages dropped to 1 keV, the entire tested area appears dark, but the contrast cannot be built effectively for distinguishing the un-affected area. In this case, even though it is possible that the transfer film can be present in the form of a few nanometres thick and less, the identification is beyond the SEM's capability. The 5 keV therefore can be regarded as an 'optimal' accelerating voltage for analysing the tested surface in this study as it unveils most of the PTFE transfer film with sufficient contrast.

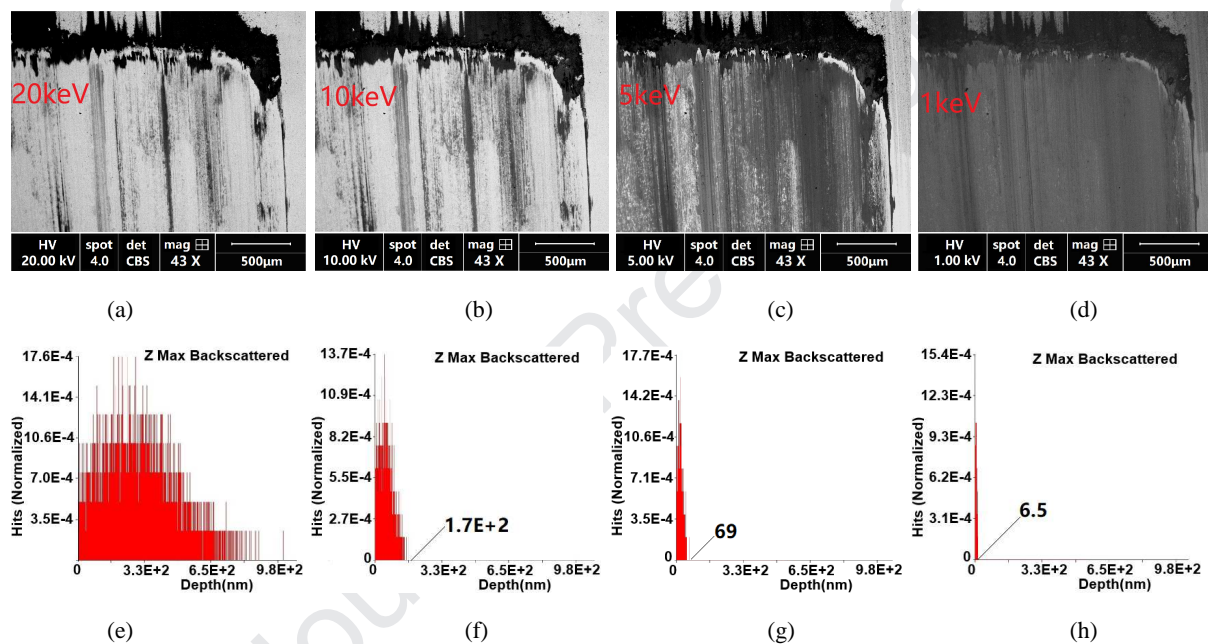


Fig. 11. BSE images of smooth (non-textured) steel counter-surface using accelerating voltage (a) 20KeV, (b) 10KeV, (c) 5KeV, and (d) 1KeV; the Depth Distribution Function graph of the BSE images using accelerating voltage (a) 20KeV, (b) 10KeV, (c) 5KeV, and (d) 1KeV

With the above two series of analysis on the PTFE transfer film, our new method of characterising transfer film reveals two distinctive forms of PTFE transfer film on the counter-surface: one at one to two micro-meters; the other in tens of nanometres and below. Because of the importance of matching the topographic variations of the counter-surface with the dimensions of the transfer film, this finding opens up a new prospect: improving transfer film formation by using micrometre-degree surface textures, while research on improving surface roughness (nanometre degree in engineering surfaces) has reached its ceiling nowadays.

3.2.2 Transfer film analysis: Towards understanding of textured counter-surfaces

Taking advantage of the new method to characterise the transfer film, SEM analysis using the optimised voltage (5 keV) has been used to evaluate transfer film's formation, including its coverage, thickness and morphology, aspects which are strongly linked with the performance of dry-lubrication.

First of all, for all the tested surfaces with Type A (wide & deep) dimples, the SEM analysis reveals that they pose a negative influence on the transfer film's coverage as presented in **Fig. 12(a)**. Taking the one with medium coverage (1.6%) as an example, from the run-in to the steady stage, the dimples always create blank strips (area 1 and area 2 in **Fig. 12**) among the film-covered area, exposing the metallic surface. This obstruction on transfer film formation appears along the sliding direction and is common in all different dimple coverages. Such an observation is in line with that Type A (wide & deep) dimples in all coverages generates negative influence on the wear performance as stated in the last section (**Fig. 5**).

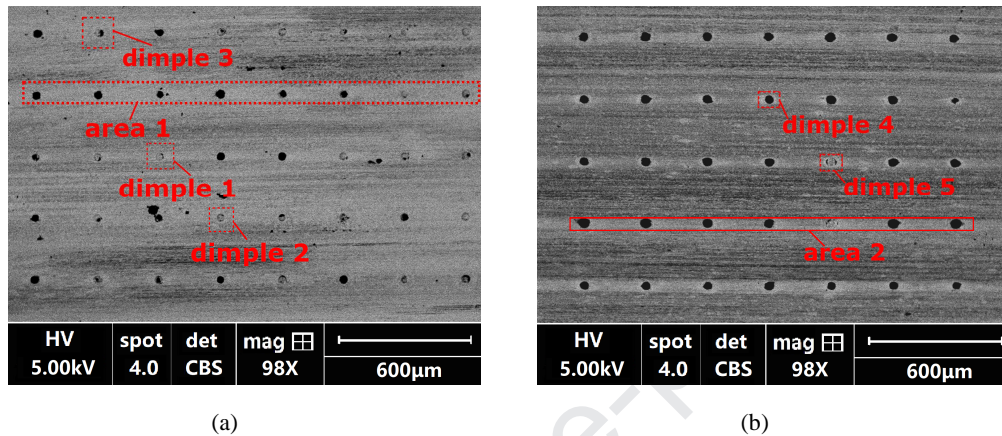
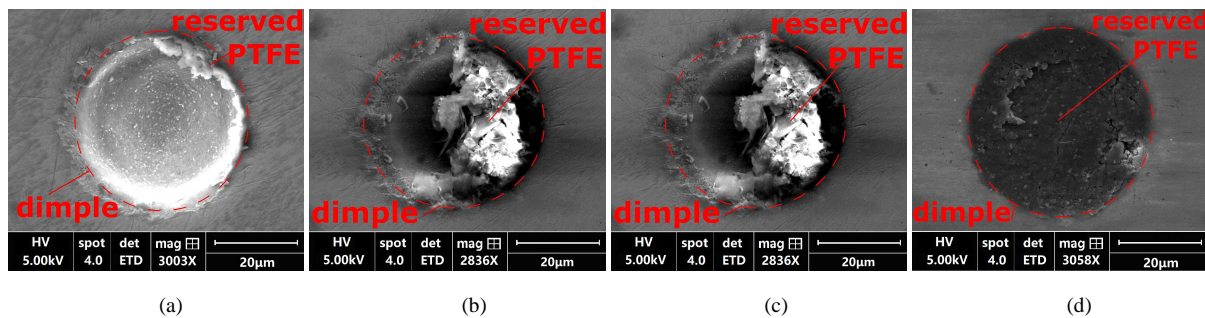


Fig. 12. BSE images of the textured counter-surface with medium coverage (1.6%) of Type A (wide & deep) dimples in (a) run-in stage and (b) steady wear stage.

With a higher magnification on the dimples 1, 2 and 3 marked in **Fig. 12**, it can be seen that the transferred PTFE was firstly obtained on the dimple's edges, as shown in **Fig. 13(e)-(g)**. The transferred debris' morphology, which is more distinguishable in SE images (**Fig. 13**), is one of rough, irregular-shaped smears- a typical indication of abrasion wear. In the steady wear stage, in most dimples contained debris has seemingly filled them, as the marked dimple 4 shown in **Fig. 13(d)** and (h). Nevertheless, in the end it could not form an integrated transfer layer outside the dimple, thus still leaving the blank strips. Moreover, small amounts of un-filled dimples still have been found, with clearly scratched debris on the edges, such as the dimple 5 marked in **Fig. 12**.



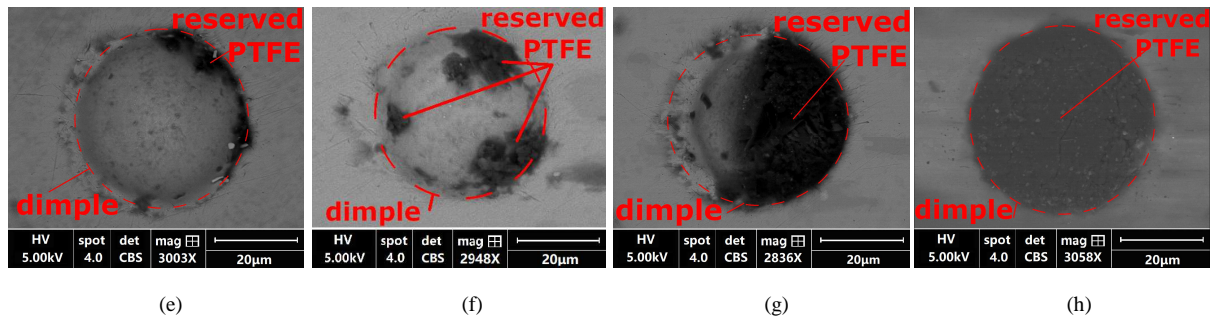


Fig. 13. (a)- (d) SE images of Type A (wide & deep) dimples from run-in to steady stage (area 1-4 marked in Fig. 12), (e)-(h) BSE images of Type A (wide & deep) dimples from run-in to steady stage (area 1-4 marked in Fig. 12).

In comparison, with the same medium coverage (1.6%), the Type B (narrow & shallow) dimples can increase the film-covered area as they create dark strips like shown in the boxed areas 1-4 in **Fig. 14**. Besides, the reserved debris are no longer rough irregular particles peeled by the edges, but smooth flakes contained on the bottom of the dimples initially, as shown in **Fig. 15** (a) and (b). This morphology feature is either from the adhesion wear of the PTFE dragged from outside the dimples, or from delamination of the composite asperities intruding into the dimple. In later stage, the reserved debris accumulate and form a transfer sheet layer. Different from the one in the wide, deep dimples, the accumulated debris can actually fill out the dimple and integrate with the transfer film formed outside the textured area in the later stage, as shown **Fig. 15** (c) and (d).

These observations prove that the dimples can act as dry-lubricants' reservoir. More importantly, the reserved debris of dry-lubricant can replenish the non-textured part of the steel surface, benefiting both the coverage and the thickness of the dry-lubricant transfer film. This phenomenon should be able to reduce the direct contact between the metallic surface with the composite liner surface, reducing both the friction and wear. Such an effect should be the key reason for the superior performance of the narrow & shallow dimples under certain coverages.

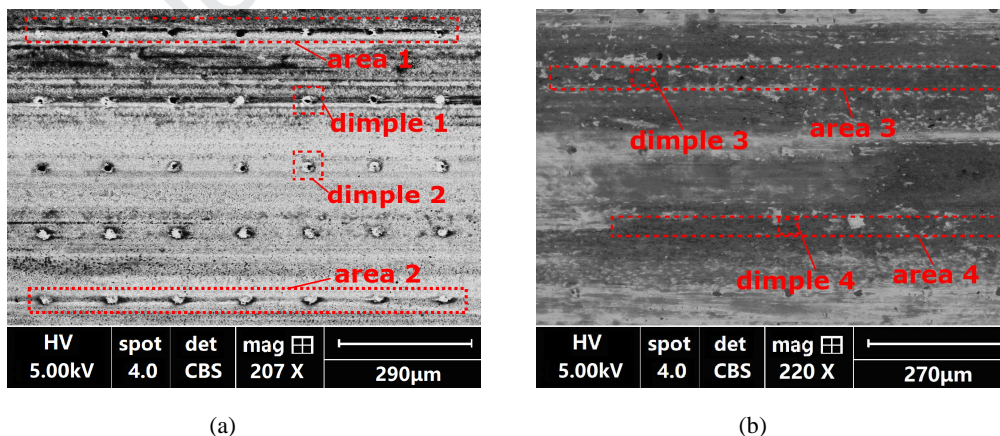


Fig. 14. BSE images of the steel counter-surface textured with medium coverage (1.6%) of Type B (narrow & shallow) dimples in (a) run-in stage and (b) steady wear stage.

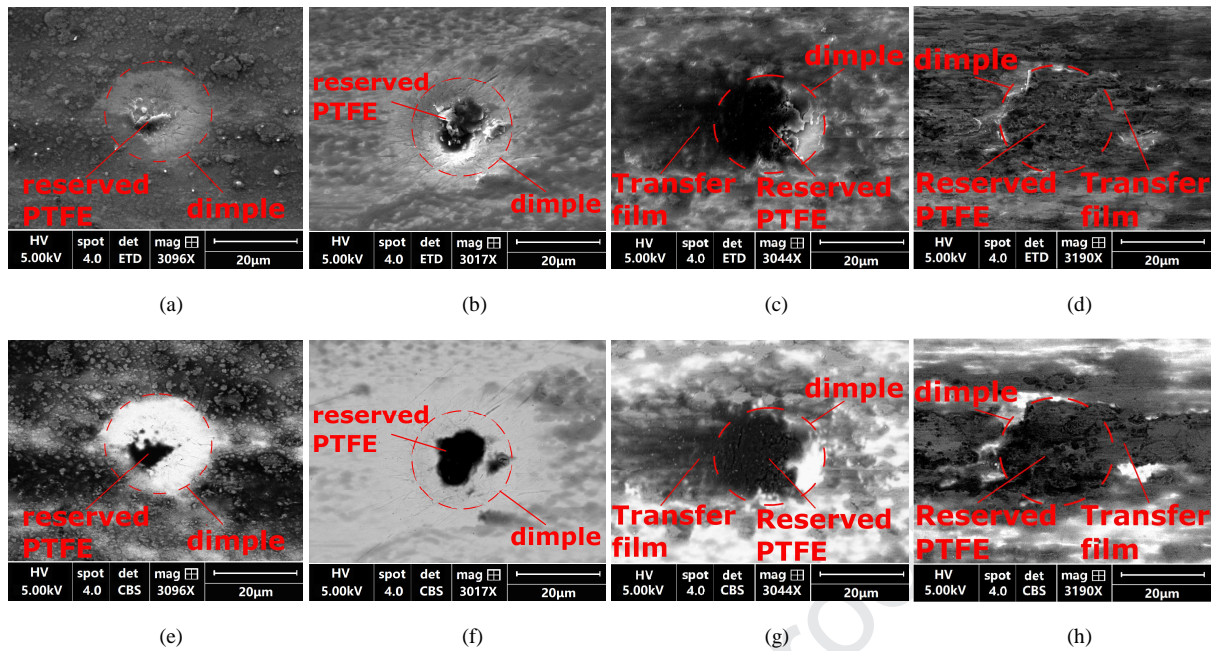


Fig. 15. (a)- (d) SE images of Type B (narrow & shallow) dimples from run-in to steady stage (area 1-4 marked in Fig. 14); (e)-(h) BSE images of Type B (narrow & shallow) dimples from run-in to steady stage (area 1-4 marked in Fig. 14).

Similarly, when the dimples are shallow yet wider (Type C) these enhanced transfer strips can also be incurred as shown in the area 1,2 and 4 in **Fig. 16(a)** and (b). However, the appearance is less common than with Type B (narrow & shallow) dimples. From the images focusing on single dimples (**Fig. 17(a)** and (b)), it was found that the Type C (wide & shallow) dimples resemble the Type A (wide & deep) dimples during the initiation of the wear process as the debris is again firstly collected on the dimples' edges. However, because it has a lower depth, which is within the range which transfer layer can form naturally on a smooth surface, the accumulated debris can build up a transfer sheet covering the dimple's depth as shown in **Fig. 17(c)** and (d) in the steady stage. Similar with the Type B (narrow & shallow) dimples, the reserved debris in these micro-holes can also form a layer integrated with the transfer film formed outside the dimple. Meanwhile, the obstruction of the transfer film, which is similar with the ones with Type A (wide & deep) dimples can also occur, such as the area 2 marked in **Fig. 16(b)**. Since both the film-thickening effect and abrasion effect are significant under these conditions, they may offset each other, and this may explain why it does not create the advantages like narrow & shallow dimples, but would not lead to apparent disadvantage like wide & deep dimples.

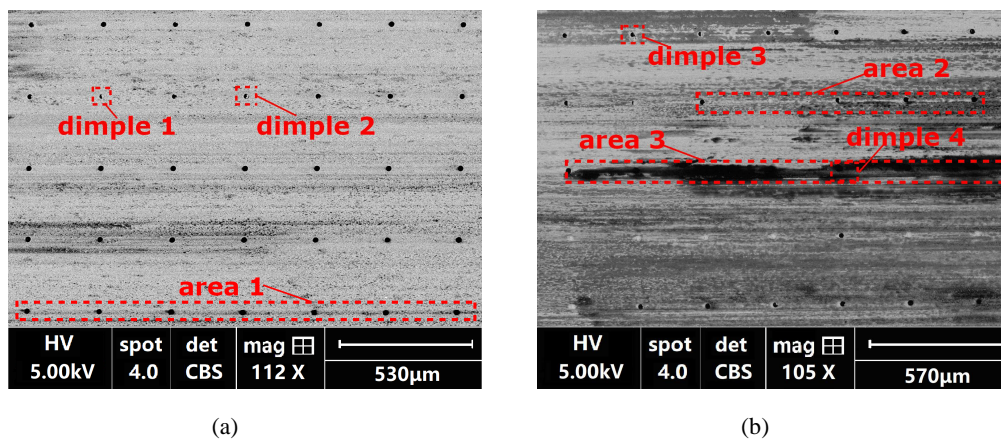


Fig. 16. BSE images of the steel counter-surface textured with medium coverage (1.6%) of Type C (wide & shallow) dimples in (a) run-in stage and (b) steady wear stage.

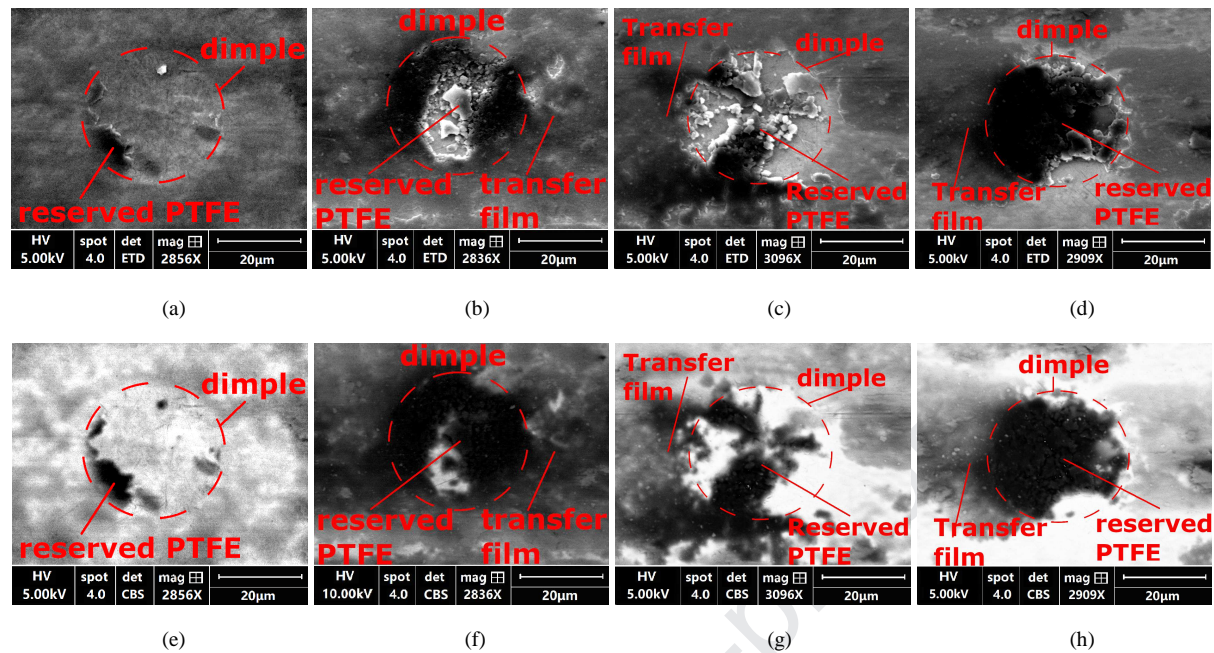


Fig. 17. (a)- (d) SE images of Type B (narrow & shallow) dimples from run-in to steady stage (area 1-4 marked in Fig. 16); (e)-(h) BSE images of Type B (narrow & shallow) dimples from run-in to steady stage (area 1-4 marked in Fig. 16).

Both of the effects summarised above are also dependant on the coverage of the dimples. For instance, with the low coverage (0.4%) of Type B (narrow & shallow) dimples, the strips of transfer film formed by dimples along sliding direction occur less occasionally. The only strip (area 1) observed in **Fig. 18** is also dis-continuous, indicating that the adjacent dimples are arranged too far apart (280 μm for low (0.4%) coverage) for the retained PTFE in the reservoirs (dimples) to travel and cover the whole distance. Moreover, with the low coverage (0.4%) of wide & shallow dimples, such a strip almost never appear (**Fig. 18(b)**). This difference should be explained by the even longer distance (560 μm) between adjacent dimples for Type C (wide & shallow) under the same coverage in comparison with the Type B (narrow & shallow).

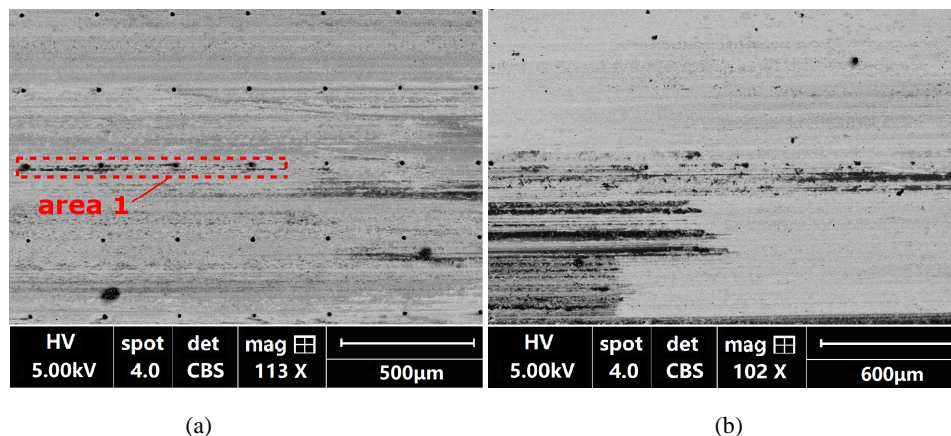


Fig. 18. BSE images of the steel counter-surface textured with low coverage (0.4%) of (a) Type B (narrow & shallow) and (b) Type C (wide & shallow) dimples in steady wear stage.

When the coverage is set as high (6.4%), however, the abrasion effect becomes more dominating for both Type B (narrow & shallow) and Type C (wide & shallow) dimples, like

shown in **Fig. 19**(a) and (b). As a result, the overall influence on transfer film is similar with the Type A (wide & deep) dimples. Therefore, it can be seen that both the coverage and dimensions of the dimples need to be on the lower side to avoid this abrasion effect. Moreover, this phenomenon is likely to be related with a more prominent increase in contact stress with higher coverage or larger size of texturing. To give a more detailed analysis of the relationship between the dimple dimensions and this effect, a finite element (FE) analysis is performed in the next section.

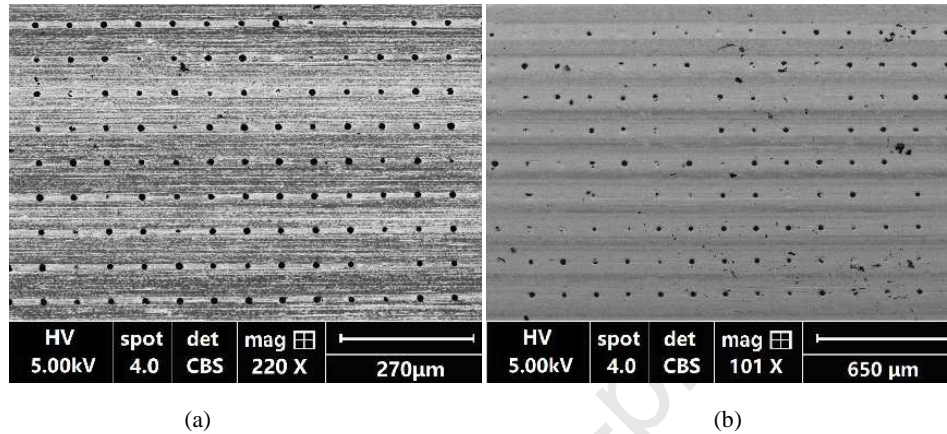


Fig. 19. BSE images of the steel counter-surface textured with high coverage (6.4%) of (a) Type B (narrow & shallow) and (b) Type C (wide & shallow) dimples in steady wear stage.

To summarize, as shown in Table 2, only with low (0.4%) and medium coverage (1.6%) of Type B (narrow & shallow) dimples will the benefit from texturing on the transfer film formation reach the high level, while the detrimental abrasion effect maintains at a lower degree. Given that the observed phenomenon (wear debris and transfer film's formation) is in line with the wear and frictional performance shown in the section 3.1, it can be deduced that both the benefiting effect on transfer film and the abrasion effect need to be considered when the surface texturing's coverage and dimensions are to be designed.

Table 2. Summary of dimple's effects in different dimensions and densities

	Type A (Wide & deep)			Type B (Narrow & shallow)			Type C (Wide & shallow)		
	Low (0.4%)	Medium (1.6%)	High (6.4%)	Low (0.4%)	Medium (1.6%)	High (6.4%)	Low (0.4%)	Medium (1.6%)	High (6.4%)
Improving film formation ^a	+	+	+	++	+++	+	+	+++	+
Abrasion ^a	++	+++	+++	+	++	+++	+	+++	+++

^a “+” means very low and “+++” means very significant effect

3.3 FE analysis to support the explanations of the influence of textured counter-surface

The FE analysis is done to study the stress strain of the composite sliding against the dimpled surfaces, covering all tested dimple dimensions and coverages to relate the observed abrasion effects with the theoretical analysis.

The first finding of the FE analysis is the stress concentration occurring in adjacent with the edges of the dimples (e.g. see circled zones in Fig. 20). As shown in **Fig. 20**(a), even with Type B (narrow & shallow) dimples, the maximum stress can reach 92.55 MPa in static condition (without sliding simulated), while with the smooth counter-surface, this value is

only 60 MPa. Succeeding with the steady state, the maximum stress can increase to 96.52 MPa at the start-up of the sliding, then stabilise at 98.42 MPa, as presented in **Fig. 20**(b) and (c).

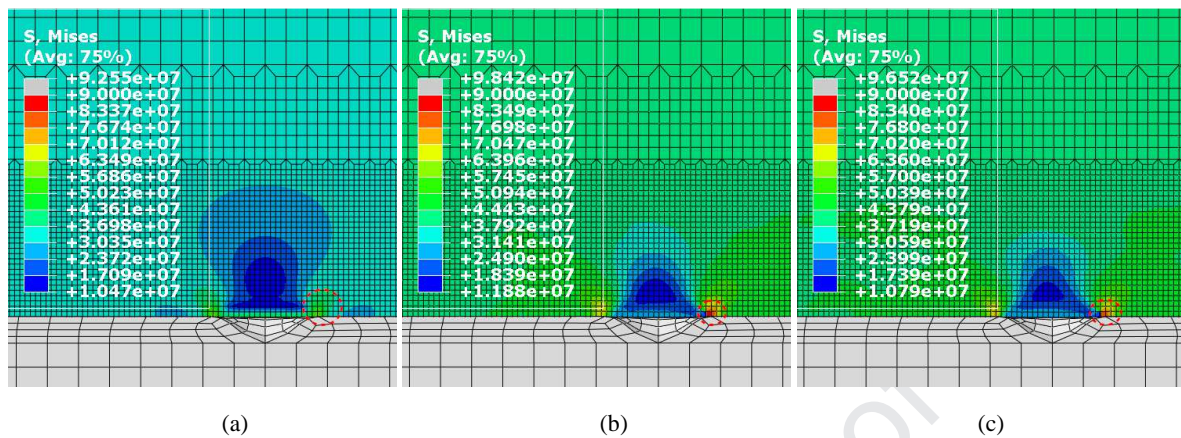


Fig. 20. Stress distribution in PTFE composite sliding against steel surface with medium coverage (1.6%) of Type B (narrow & shallow) dimples at (a) start of the sliding (b) first step of sliding (c) steady state of sliding.

Furthermore, the higher the dimple coverage the more severe the stress concentration is at the edges of the micro-cavities. As the example presented in **Fig. 21**(a) to (c), the maximum contact stress at the stabilised stage is correspondingly 3.93 and 5.87 MPa higher in medium and high coverage than low coverage.

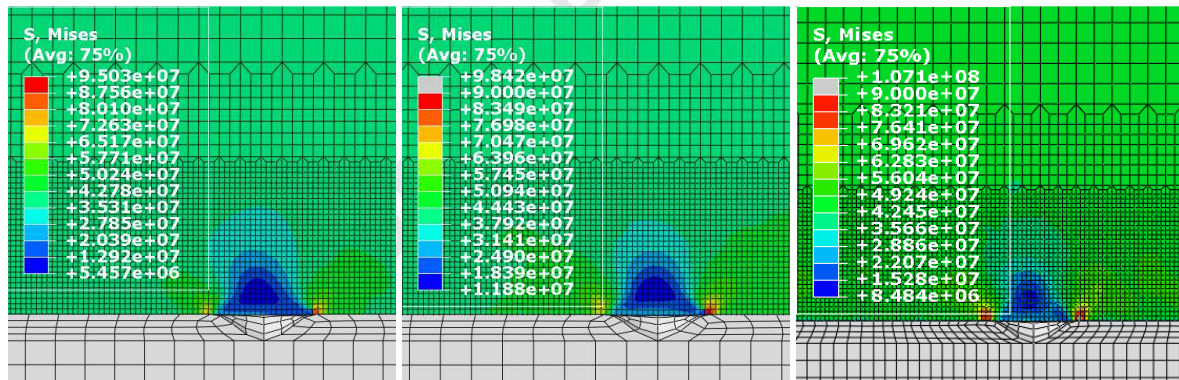


Fig. 21. Steady-state stress distribution in PTFE composite sliding against steel surface with narrow & shallow dimples in (a) low coverage (0.4%), (b) medium coverage (1.6%) and (c) high coverage (6.4%)

Moreover, dimple dimensions also play a crucial role. As shown in **Fig. 22**, at low coverage, the maximum stress with (Type A) wide & deep dimples and (Type C) wide & shallow dimples can reach 133.1 MPa and 111.1 MPa, dramatically higher than the (Type B) narrow & shallow dimples.

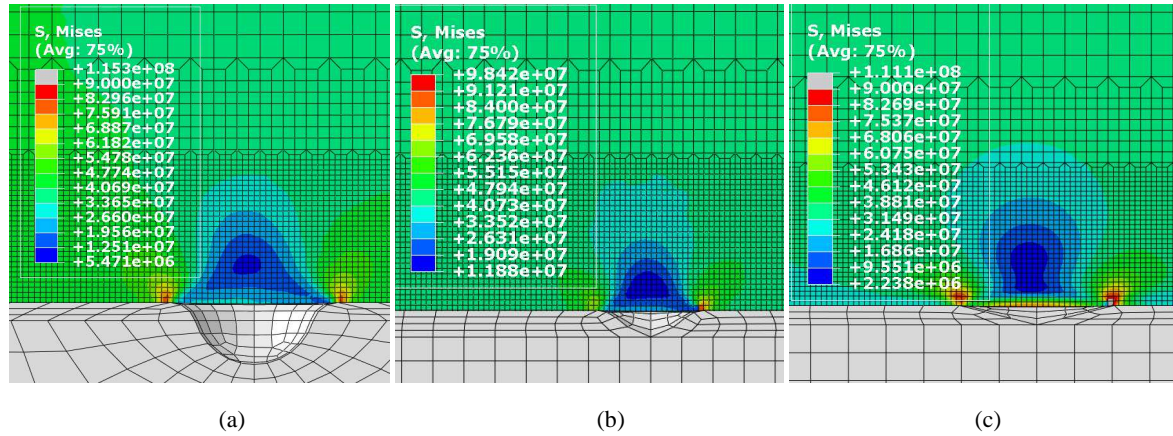


Fig. 22. Steady-state stress distribution in PTFE composite sliding against steel surface with medium coverage (1.6%) of (a) Type A (wide & deep) dimples, (b) Type B (narrow & shallow) dimples and (c) Type C (wide & shallow) dimples

From the summarising graph (**Fig. 23**), both the maximum contact stress (σ_{max}) and percent of plastically deformed elements ($p_{ep>0}$) rise with the increase of coverage. Moreover, both parameters for Type A (wide & deep) and Type C (wide & shallow) dimples are close, but significantly higher than Type B (narrow & shallow) dimples in each coverage. Essentially, larger diameter and higher coverage would lead to aggravated stress concentration and plastic deformations, while the depth of the dimples plays a negligible role. Relating this finding with the observed abrasion effects in different dimensions (shown in Table 2), it can be seen that the maximum stress and plastic strain give a good indication for level of abrasion effects (the second row of Table 2). If the diameter and coverage of the dimples are designed to be in a lower range low enough, minimal proportion (under 2% in this instance) of the softer composite surface would experience high stress concentration (i.e. above the yield strength 100 MPa in this example), and the abrasion effect would efficiently be maintained mild. On the contrary, if the textures are designed so that a substantial volume (over 5% in this case) of the composite part would deform plastically, significant abrasion effect would occur. Overall, this FE analysis provides the rationale why the dimensions (particularly the diameter) and coverage of the dimples should be constrained in the narrow range found to avoid significant abrasion effect.

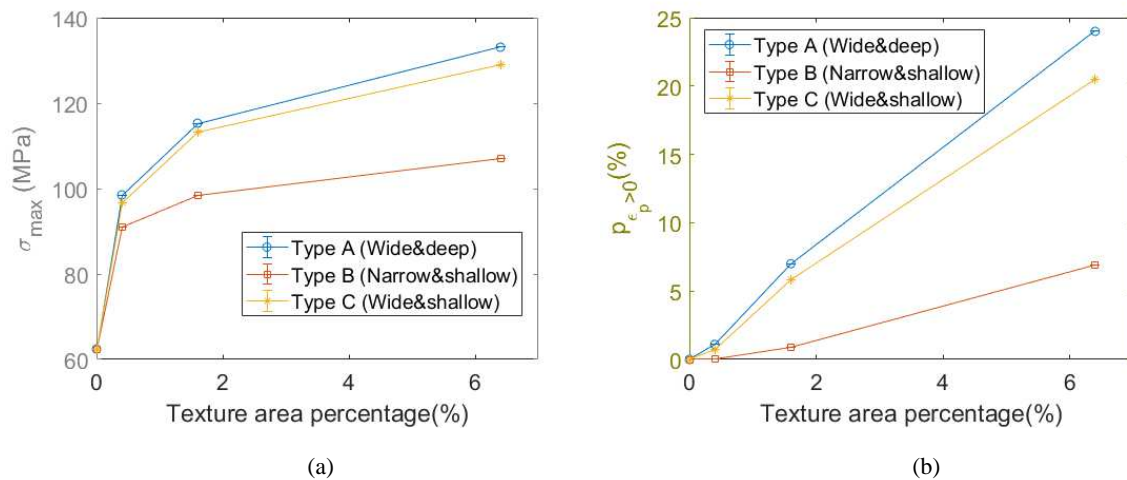


Fig. 23. (a) Maximum contact stress and (b) percentage of surface elements under plastic deformation on the composite surface sliding against steel surface textured with different types of dimples in different coverages at steady state

4 Conclusion

This paper reports on the understanding of the transfer film formation of dry lubricant with the presence of hard reinforcing fibres. With the obtained knowledge, the phenomena governing the composite's frictional and wear performance sliding against textured counter-surface have been discovered, relating with the different wear mechanisms experienced with dimples in varied coverages and dimensions.

Through analysing the transfer film by layers with SEM in different accelerating voltages (with Tof-SIMS as an assisting technique), transfer film's dimensional properties is established- two forms of transfer film coexist on the steel surface: the ultra-thin film (nano-meter degree) and the thicker transfer layer (micro-meter degree).

Through wear tests, it was found the surface texturing may benefit the formation of the thicker form of transfer film, and the key is to constrain the dimple depth (dep) within the magnitude of the film thickness ($2\sim 3\ \mu\text{m}$). Moreover, there is a very narrow window of the dimples' diameters and densities ($d\leq 20\ \mu\text{m}$, $p_c\leq 1.6\%$) for the effect to be achieved without incurring significant micro-abrasion, since severe stress concentration (exceeding the composite's yield strength as revealed by FE) can occur near the dimple edges.

Although the obtained results may have their limitation on this particular tribo-pair material, the strategy of transfer film characterisation and the observed effects with textured counter-surface can be applicable in similar dry-sliding contact.

Acknowledgments

Funding: This work was supported by SKF UK. Ltd and Marie Skłodowska-Curie actions (project number ENG969). The authors are grateful to the support provided, and particularly the technical advice from Mr. Michael Colton and Dr. Johnpaul Woodhead in SKF UK. Ltd.

Reference

- [1] D.C. Evans, G.S. Senior, Self-lubricating materials for plain bearings, *Tribol. Int.* 15 (1982) 243–248. [https://doi.org/https://doi.org/10.1016/0301-679X\(82\)90077-9](https://doi.org/https://doi.org/10.1016/0301-679X(82)90077-9).
- [2] S. Raadnui, S. Mahathanabodee, R. Tongtong, Tribological behaviour of sintered 316L stainless steel impregnated with MoS₂ plain bearing, *Wear.* 265 (2008) 546–553. <https://doi.org/10.1016/j.wear.2007.11.014>.
- [3] A. Wang, A. Essner, V.K. Polineni, C. Stark, J.H. Dumbleton, Lubrication and wear of ultra-high molecular weight polyethylene in total joint replacements, in: *Tribol. Int.*, 1998. [https://doi.org/10.1016/S0301-679X\(98\)00005-X](https://doi.org/10.1016/S0301-679X(98)00005-X).
- [4] Russell Gay, *FRICITION AND WEAR BEHAVIOUR OF SELF LUBRICATING BEARING LINERS* Thesis submitted in candidature for the degree of Doctor of Philosophy at Cardiff University Tribology Group Institute of Theoretical , Applied and Computational Mechanics Cardiff School of En, Cardiff University, 2013.
- [5] T.A. Blanchet, F.E. Kennedy, Sliding wear mechanism of polytetrafluoroethylene (PTFE) and PTFE composites, *Wear.* 153 (1992) 229–243. [https://doi.org/10.1016/0043-1648\(92\)90271-9](https://doi.org/10.1016/0043-1648(92)90271-9).
- [6] S.K. Biswas, K. Vijayan, Friction and wear of PTFE, *Wear.* 158 (1992) 193–211. [https://doi.org/10.1016/0043-1648\(92\)90039-B](https://doi.org/10.1016/0043-1648(92)90039-B).
- [7] J. Ye, D.L. Burris, T. Xie, A Review of Transfer Films and Their Role in Ultra-Low-Wear Sliding of Polymers, (2016) 1–15. <https://doi.org/10.3390/lubricants4010004>.
- [8] W. Wieleba, The statistical correlation of the coefficient of friction and wear rate of PTFE composites with steel counterface roughness and hardness, *Wear.* 252 (2002) 719–729. [https://doi.org/10.1016/S0043-1648\(02\)00029-7](https://doi.org/10.1016/S0043-1648(02)00029-7).
- [9] J.K. Lancaster, Accelerated wear testing as an aid to failure diagnosis and materials selection, *Tribol. Int.* 15 (1982) 323–329. [https://doi.org/10.1016/0301-679X\(82\)90141-4](https://doi.org/10.1016/0301-679X(82)90141-4).
- [10] P.L. Menezes, S.V. Kailas, Role of surface texture and roughness parameters on friction and transfer film formation when UHMWPE sliding against steel, *Biosurface and Biotribology.* 2 (2016) 1–10. <https://doi.org/10.1016/j.bsbt.2016.02.001>.
- [11] C.M. Pooley, D. Tabor, Friction and Molecular Structure: The Behaviour of Some Thermoplastics, *Proc. R. Soc. A Math. Phys. Eng. Sci.* 329 (1972) 251–274. <https://doi.org/10.1098/rspa.1972.0112>.
- [12] J.L. Lauer, B.G. Bunting, W.R. Jones Jr, Investigation of PTFE transfer films by infrared emission spectroscopy and phase-locked ellipsometry, (1987).
- [13] K.R. Makinson, D. Tabor, The friction and transfer of polytetrafluor ethylene, 281 (1964).

- [14] G. Beamson, D.T. Clark, D.E. Deegan, N.W. Hayes, D.S.L. Law, J.R. Rasmusson, W.R. Salaneck, Characterization of PTFE on silicon wafer tribological transfer films by XPS, imaging XPS and AFM, *Surf. Interface Anal.* 24 (1996) 204–210. [https://doi.org/10.1002/\(SICI\)1096-9918\(199603\)24:3<204::AID-SIA90>3.0.CO;2-C](https://doi.org/10.1002/(SICI)1096-9918(199603)24:3<204::AID-SIA90>3.0.CO;2-C).
- [15] X. Lu, K.C. Wong, P.C. Wong, K.A.R. Mitchell, J. Cotter, D.T. Eadie, Surface characterization of polytetrafluoroethylene (PTFE) transfer films during rolling-sliding tribology tests using X-ray photoelectron spectroscopy, *Wear.* 261 (2006) 1155–1162. <https://doi.org/10.1016/j.wear.2006.03.020>.
- [16] J. Khedkar, I. Negulescu, E.I. Meletis, Sliding wear behavior of PTFE composites, *Wear.* 252 (2002) 361–369. [https://doi.org/10.1016/S0043-1648\(01\)00859-6](https://doi.org/10.1016/S0043-1648(01)00859-6).
- [17] Z. Zuo, Y. Yang, X. Qi, W. Su, X. Yang, Analysis of the chemical composition of the PTFE transfer film produced by sliding against Q235 carbon steel, *Wear.* 320 (2014) 87–93. <https://doi.org/10.1016/j.wear.2014.08.019>.
- [18] I. Minami, T. Kubo, H. Nanao, S. Mori, H. Iwata, M. Fujita, Surface Chemistry for Improvement in Load-Carrying Capacity of Poly (Ether-Ether-Ketone) -Based Materials by Poly (Tetrafluoroethylene), 3 (2008) 190–194. <https://doi.org/10.2474/trol3.190>.
- [19] J.I. Goldstein, D.E. Newbury, J.R. Michael, N.W.M. Ritchie, J.H.J. Scott, D.C. Joy, Scanning electron microscopy and x-ray microanalysis, 2017. <https://doi.org/10.1007/978-1-4939-6676-9>.
- [20] H. Singh, K.C. Mutyala, R.D. Evans, G.L. Doll, An investigation of material and tribological properties of Sb₂O₃/Au-doped MoS₂ solid lubricant films under sliding and rolling contact in different environments, *Surf. Coatings Technol.* (2015). <https://doi.org/10.1016/j.surfcoat.2015.05.049>.
- [21] W.J.A. Hamilton D. B., C.M. Allen, A Theory of Lubrication by Micro-asperities, *ASME J. Basic Eng.* 88(1) (1966) 177–185.
- [22] A. Greco, S. Raphaelson, K. Ehmann, Q.J. Wang, C. Lin, Surface texturing of tribological interfaces using the vibromechanical texturing method, *J. Manuf. Sci. Eng. Trans. ASME.* (2009). <https://doi.org/10.1115/1.4000418>.
- [23] Q. Ding, L. Wang, Y. Wang, S.C. Wang, L. Hu, Q. Xue, Improved tribological behavior of DLC films under water lubrication by surface texturing, *Tribol. Lett.* 41 (2011) 439–449. <https://doi.org/10.1007/s11249-010-9730-1>.
- [24] K.Y. Etsion I., G. Halperin, Analytical and Experimental Investigation of Laser-Textured Mechanical Seal Faces, *Tribol. Trans.* 42 (1999) 511–516.
- [25] N. Saka, H. Tian, N.P. Suh, Boundary Lubrication of Undulated Metal Surfaces at Elevated Temperatures, *Tribol. Trans.* 32 (1989) 389–395. <https://doi.org/10.1080/10402008908981904>.
- [26] H. Tian, N. Saka, N.P. Suh, Boundary Lubrication Studies on Undulated Titanium

- Surfaces, Tribol. Trans. 32 (1989) 289–296.
<https://doi.org/10.1080/10402008908981891>.
- [27] C. Gachot, A. Rosenkranz, L. Reinert, E. Ramos-Moore, N. Souza, M.H. Müser, F. Mücklich, Dry friction between laser-patterned surfaces: Role of alignment, structural wavelength and surface chemistry, *Tribol. Lett.* 49 (2013) 193–202.
<https://doi.org/10.1007/s11249-012-0057-y>.
- [28] C. Gachot, A. Rosenkranz, S.M. Hsu, H.L. Costa, A critical assessment of surface texturing for friction and wear improvement, *Wear.* 372–373 (2017) 21–41.
<https://doi.org/10.1016/j.wear.2016.11.020>.
- [29] Q. Sun, T. Hu, H. Fan, Y. Zhang, L. Hu, Dry sliding wear behavior of TC11 alloy at 500°C: Influence of laser surface texturing, *Tribol. Int.* 92 (2015) 136–145.
<https://doi.org/10.1016/j.triboint.2015.06.003>.
- [30] B. Zhang, W. Huang, J. Wang, X. Wang, Comparison of the effects of surface texture on the surfaces of steel and UHMWPE, *Tribol. Int.* 65 (2013) 138–145.
<https://doi.org/10.1016/j.triboint.2013.01.004>.
- [31] D. He, S. Zheng, J. Pu, G. Zhang, L. Hu, Improving tribological properties of titanium alloys by combining laser surface texturing and diamond-like carbon film, *Tribol. Int.* (2015). <https://doi.org/10.1016/j.triboint.2014.09.017>.
- [32] M. Wang, C. Zhang, X. Wang, The wear behavior of textured steel sliding against polymers, *Materials (Basel)*. 10 (2017). <https://doi.org/10.3390/ma10040330>.
- [33] D. Gu, C. Duan, B. Fan, S. Chen, Y. Yang, Tribological properties of hybrid PTFE/Kevlar fabric composite in vacuum, *Tribol. Int.* 103 (2016) 423–431.
<https://doi.org/10.1016/j.triboint.2016.08.004>.
- [34] F. Kennedy, L. Smidhammar, D. Play, Wear of polyethylene in small-amplitude oscillatory motion., (1985).
- [35] K. Li, X. Shen, Y. Chen, R. Li, Numerical Analysis of Woven Fabric Composites Lubricated Spherical Plain Bearings, *Proc. XIth Int. Congr. Expo.* (2008). <http://sem-proceedings.com/08s/sem.org-SEM-XI-Int-Cong-s076p04-Numerical-Analysis-Woven-Fabric-Composites-Lubricated-Spherical.pdf>.
- [36] A.I. Aguilar-Morales, S. Alamri, A.F. Lasagni, Micro-fabrication of high aspect ratio periodic structures on stainless steel by picosecond direct laser interference patterning, *J. Mater. Process. Technol.* (2018). <https://doi.org/10.1016/j.jmatprotec.2017.09.039>.
- [37] A. Ancona, S. Döring, C. Jauregui, F. Röser, J. Limpert, S. Nolte, A. Tünnermann, Femtosecond and picosecond laser drilling of metals at high repetition rates and average powers, *Opt. Lett.* 34 (2009) 3304. <https://doi.org/10.1364/ol.34.003304>.
- [38] X. Fang, C. Zhang, X. Chen, Y. Wang, Y. Tan, Newly developed theoretical solution and numerical model for conformal contact pressure distribution and free-edge effect in spherical plain bearings, *Tribol. Int.* 84 (2015) 48–60.

<https://doi.org/10.1016/j.triboint.2014.11.020>.

Journal Pre-proof

Highlights:

- Addressed the issue with characterising PTFE transfer film on the counter-surface with wear tracks for the first time
- Developed a novel approach for characterising PTFE transfer film using SEM incorporated with Time-of-Flight Secondary Ion Mass Spectrometry (ToF-SIMS) analysis
- Observed transfer film reservation and micro-abrasion on the counter-surface with varied dimensions and coverages of surface textures (dimples)
- Correlated the surface textures' influence on the PTFE composites' tribological performance with the observed phenomena

WEAR

Confirmation of Authorship

Please save a copy of this MS Word file, complete and upload as the “Confirmation of Authorship” file.

As corresponding author, I, Dragos Axinte, hereby confirm on behalf of all authors that:

- 1) The authors have obtained the necessary authority for publication.
- 2) The paper has not been published previously, that it is not under consideration for publication elsewhere, and that if accepted it will not be published elsewhere in the same form, in English or in any other language, without the written consent of the publisher.
- 3) The paper does not contain material which has been published previously, by the current authors or by others, of which the source is not explicitly cited in the paper.

Upon acceptance of an article by the journal, the author(s) will be asked to transfer the copyright of the article to the publisher. This transfer will ensure the widest possible dissemination of information.

Declaration of interests

The authors declare that they have no known competing financial interests or personal relationships that could have appeared to influence the work reported in this paper.

The authors declare the following financial interests/personal relationships which may be considered as potential competing interests:

Journal Pre-proof